Shahnazian, Fatemeh; Adabi, Jafar; Pouresmaeil, Edris

Enhanced control of voltage source converters considering virtual inertia theory

Published in:
International Transactions on Electrical Energy Systems

DOI:
10.1002/2050-7038.13245

Published: 01/12/2021

Document Version
Peer-reviewed accepted author manuscript, also known as Final accepted manuscript or Post-print

Please cite the original version:
Shahnazian, F., Adabi, J., & Pouresmaeil, E. (2021). Enhanced control of voltage source converters considering virtual inertia theory. *International Transactions on Electrical Energy Systems*, *31*(12), Article 13245. https://doi.org/10.1002/2050-7038.13245

Enhanced Control of Voltage Source Converters Considering Virtual Inertia Theory

Fatemeh Shahnazian[1], Jafar Adabi[1], Edris Pouresmaeil[2]

[1] Department of Electrical and Computer Engineering, Babol Noshirvani University of Technology, Babol, Iran

[2] Department of Electrical Engineering and Automation, Alto University, Espoo, Finland

Correspondence

Jafar Adabi, Babol Noshirvani University of Technology, Babol, Iran

Email: j.adabi@nit.ac.ir

Summary: This paper presents an enhanced control strategy for voltage source converters (VSCs) based on virtual inertia concept. Considering the significant share of renewable-based generations, frequency stability is noted as one of the most significant challenges of modern low-inertia power systems. Therefore, as the first contribution of this paper, dynamic equations of the converter are utilized in order to study its proficient active and reactive power compensation capabilities. Then, this effective power factor correction of the proposed VSC is improved by adding inertia emulation characteristics in order to provide a more synchronous generator (SG) like behavior, which is beneficial from the frequency stability point of view. In addition to that, the impacts of changes in the main control parameters such as inertia and damping on dynamic performance are analyzed using the root locus method. This applied eigenvalue analysis has then been used to support a proper selection of parameter values, which is considered as another novelty of this paper. In this regard, the designed algorithm providing auto adjustment capability of controller parameters based on a desired frequency response characteristic can improve the dynamic frequency stability of the system. The functionality of the proposed controller is validated through state-space analysis and simulations with MATLAB/Simulink. The superior performance of the proposed algorithm demonstrated through simulation results confirms that the proposed control method can be considered as a simple yet effective solution for the challenges of a reduced inertia power system.

KEYWORKS: Inertia emulation, renewable energy sources, virtual synchronous generator, voltage source converter (VSC).

1. INTRODUCTION

Modern power systems are mostly moving towards using renewable energy sources (RESs) as their main power suppliers. The global demand for environmentally friendly and clean energy sources has made RESs a promising horizon for the future power grid.[1] The power can be achieved from different kinds of RESs such as wind power, photovoltaic, and fuel-cells. Therefore, distributed generators (DGs) are usually interfaced through various power electronic components such as voltage source converters (VSCs).[2] In this regard, increased penetration of renewable energy resources has led to a more converter-dominant power grid and thus, properly designed and tuned control methods are of great importance in order to achieve appropriate power system operation.[3]

With that in mind, several control strategies have been proposed in order to improve the operation quality of the interconnected VSCs.[4] Various control objectives including technical, economical, and environmental aspects are addressed in the literature.[5] Reference 6 provides an overview of different control approaches and synchronization methods for grid-forming converters. Various harmonic mitigation methods in microgrids[7], maximum power transfer capability for the grid-connected converters, and transient stability enhancement under weak-grid conditions have also been addressed in the literature.[8,9] In spite of all the above-mentioned strategies, there still seems to be a need to design a practical multi-objective controller which considers various purposes while integrating RESs into the power grid.[5] Reference 10 proposes such a multi-purpose control strategy which compensates load active and reactive power components along with the harmonic currents. Using the proposed method, VSC can control the active power injection from DG to grid. Moreover, load reactive power and harmonic current components will be compensated, leading to a sinusoidal grid current and a unity power factor. The proposed control method decouples active and reactive current components and provides fast dynamic responses while tracking the active and reactive power references.[10]

Although using inverter interfaced RESs with such a valuable control strategy can be very advantageous from many aspects, recent studies have reported a significant concern about frequency stability issues.[11] The problem manifests itself since the proposed controllers of inverter interfaced RESs do not provide any kind of inertial response for the system.[12] Accordingly, the compromised frequency stability leads to a strong need for additional studies on virtual inertia based control methods. In this regard, virtual inertia is considered as an inevitable component in the modern power grids with high penetration of RESs and therefore, several solutions have been proposed in the literature in order to solve the lack of inertial response issue.[13,14]

Latest research trends are focused on different virtual inertia emulation methods to improve the sustainability of the power systems.[15-18] Basically, droop-based control strategies can approximate the performance of virtual inertia schemes.[19,20] The most serious shortcoming is that traditional droop-based controllers are mostly capable of steady-state frequency regulations while dynamic frequency responses are of great importance as well.[21,22] One straightforward approach is to emulate the inertial response characteristics of a synchronous generator (SG) in the VSC-based interface system and create a virtual synchronous generator (VSG).[23] Reference 24 proposes an optimal design for VSGs in order to improve the transient stability of the system. Using the derivative of measured system frequency in converter swing equation, the intended dynamic frequency control is provided. The proposed inertia emulation strategy is able to represent a dynamic behavior similar to SGs in case of power imbalances without incorporating all of the detailed equations.[25,26]

On the other hand, the addition of these new control parameters makes it necessary to study their influence on dynamic performance of the controller.[27] In this regard, root locus analysis can be considered as a powerful method in order to provide valuable information about the effects of parameter changes on dynamic response of the system.[28,29] As a result, various recent studies often utilize the abovementioned eigenvalue analysis to evaluate dynamic impacts of virtual parameters on small signal stability of the system.[30] In this regard, an exhaustive modal analysis of interconnected European power system has been provided in Ref. 31 in order to find the oscillatory modes of the studied model. However, it is good to mention that these studies often use root locus as a method in order to validate a pre-designed controller's performance in the stable operation range. This is while the inherent potentials of eigenvalue analysis in providing valuable data for design seems to be often neglected so far.

This paper presents an enhanced control strategy for VSCs, based on the proposed approach in Ref. 10, which considers virtual inertia emulation in order to ensure similar frequency dynamics to SGs. This way, maximum available active power as well as reactive and harmonic current component compensations are accomplished in order to improve the grid current quality. Moreover, considering inertial response of the converter during power imbalances leads to an improved SG-similar behavior which is considered as the first novelty of this paper. In addition to that, root locus analysis has also been performed in order to study the influence of the virtual parameter variations on system stability. In this regard, a novel control structure is proposed in order to determine the accurate values of damping and inertia parameters based on this eigenvalue analysis. Therefore, this auto selection of controller parameters based on a desired characteristic of the dynamic frequency response is considered as the second contribution this paper provides. The functionality of the proposed controller is validated through state-space analysis and simulations using MATLAB/Simulink.

The rest of the paper is organized as follows. Section 2 provides a general overview of the converter structure and the applied basic control method. Section 3 describes the proposed inertia emulation control strategy along with the relevant eigenvalue analysis of the controller. The overall structure of the proposed control strategy as well as the state-space stability analysis has been represented in section 4 while the simulation results are discussed in section 5. Finally, the overall conclusions are specified in section 6.

2. GENERAL STRUCTURE AND BASIC CONTROL SCHEME OVERVIEW

The general structure of a grid connected VSC is shown in Figure 1. Considering $x=a,b,c$, i_{gx} , i_{lx} , and i_{cx} represent grid, load, and converter output currents respectively. Furthermore, R_c and L_c represent the equivalent resistance and inductance of the components between VCS and the point of common coupling (PCC). R_g and L_g also represent the equivalent resistance and inductance of the power grid.

Applying Kirchhoff's voltage law (KVL) to the structure represented in Figure 1 leads to:

$$v_x = e_x - R_c i_{cx} - L_c \frac{di_{cx}}{dt} \tag{1}$$

where, v_x and e_x represent PCC and converter output voltages respectively. Considering the switching function S_x such that:

$$S_x = \begin{cases} 1, & \text{if } s_{x1} \text{ is on and } s_{x2} \text{ is off} \\ 0, & \text{if } s_{x1} \text{ is off and } s_{x2} \text{ is on} \end{cases} \tag{2}$$

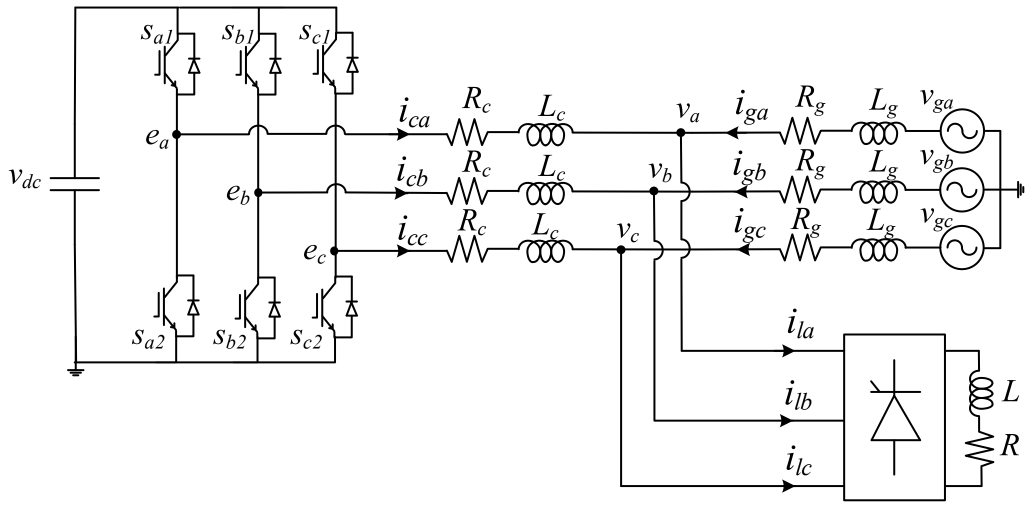

FIGURE 1. General structure of a grid-connected VSC.

we have $e_x = S_x v_{dc}$ where, v_{dc} represents the dc-link voltage. Therefore, (3) can be expressed as:

$$\frac{di_{cx}}{dt} = \frac{1}{L_c} S_x v_{dc} - \frac{R_c}{L_c} i_{cx} - \frac{1}{L_c} v_x \tag{3}$$

Equation (3) can clearly represent the dynamic behavior of the grid-connected VSC.[10] Applying Park's transformation to the above-mentioned equation while considering zero homo-polar current component leads to:

$$\frac{d}{dt}\begin{bmatrix} i_{cd} \\ i_{cq} \end{bmatrix} = \frac{1}{L_c}\begin{bmatrix} S_d \\ S_q \end{bmatrix} v_{dc} - \begin{bmatrix} \frac{R_c}{L_c} & -\omega \\ \omega & \frac{R_c}{L_c} \end{bmatrix}\begin{bmatrix} i_{cd} \\ i_{cq} \end{bmatrix} - \frac{1}{L_c}\begin{bmatrix} v_d \\ v_q \end{bmatrix} \tag{4}$$

We consider that the load voltage vector is in position with d-axis. Thus, the q-axis voltage vector becomes zero ($v_q = 0$) while, v_d equals the rms value of the grid voltage (V_g). In this regard, (5) can be expressed as:

$$\frac{d}{dt}\begin{bmatrix} i_{cd} \\ i_{cq} \end{bmatrix} = \frac{1}{L_c}\begin{bmatrix} S_d \\ S_q \end{bmatrix} v_{dc} - \begin{bmatrix} \frac{R_c}{L_c} & -\omega \\ \omega & \frac{R_c}{L_c} \end{bmatrix}\begin{bmatrix} i_{cd} \\ i_{cq} \end{bmatrix} - \frac{1}{L_c}\begin{bmatrix} V_g \\ 0 \end{bmatrix} \tag{5}$$

Consequently, the two switching state functions in dq frame can be obtained as:

$$S_d = \frac{\lambda_d - L_c \omega i_{cq} + V_g}{v_{dc}} \tag{6}$$

$$S_q = \frac{\lambda_q + L_c \omega i_{cd}}{v_{dc}} \tag{7}$$

where $\lambda = L_c \frac{di_c}{dt} + R_c i_c$. In order to have a fast accurate dynamic response with zero steady-state errors, a proportional-integral (PI) controller is used. The proposed regulator can be expressed as:

$$(\lambda_{dq}) = k_p(\Delta i_{cdq}) + \underbrace{k_i \int (\Delta i_{cdq}) dt}_{\varphi_{i_{cdq}}} \tag{8}$$

where the terms k_p and k_i represent the proportional and integral gains of the PI regulator, respectively. In addition, the error signal can be expressed as:

$$\left(\Delta i_{cdq}\right) = \left(i^*_{cdq}\right) - \left(i_{cdq}\right) \tag{9}$$

which represents a comparison between the calculated reference currents and the actual VSC output currents. Appropriate adjusting of the controller parameters leads to an accurate control on VSC switches according to the current compensation objectives. In this regard, dq components of VSC reference current should be properly calculated.

2.1 Calculation of d-Axis Reference Current

The fundamental frequency active power injected from VSC to the grid can be calculated as follows:

$$P = \frac{3}{2}\left(v_d I_{cd} + v_q I_{cq}\right) \tag{10}$$

where capital letters are used in order to represent fundamental frequency components. There is a limit to the maximum available active power delivered by each individual VSC in fundamental frequency (represented here by P_{ref}), which is considered to be fully demanded by the connected load. Therefore, considering the initial assumption of $v_q = 0$ leads to the fundamental frequency d-axis reference current expression as:

$$I^*_{cd} = \frac{2}{3}\frac{P_{ref}}{v_d} \tag{11}$$

On the other hand, there are also harmonic load current components ($\tilde{i_{ld}}$) which can be extracted using a high-pass filter (HPF) since fundamental frequency current (I_{ld}) emerges as a dc component in dq frame. Therefore, (12) can be expressed as:

$$\tilde{i_{ld}} = i_{ld} - I_{ld} \tag{12}$$

Consequently, total d-component of the VSC reference current can be achieved considering both fundamental and harmonic frequency components as:

$$i_{cd}^{*} = \tilde{i_{ld}} + I_{cd}^{*} \tag{13}$$

This way, the VSC can be effectively utilized in order to provide the maximum available fundamental frequency active power as well as the total harmonic components of the load active power demand.

2.2 Calculation of q-Axis Reference Current

The VSC is supposed to compensate total load reactive power demands, considering harmonic components as well. In this regard, q-component of VSC's reference current should be considered equal to the corresponding load current component as:

$$i_{cq}^{*} = i_{lq} \tag{14}$$

It should be noted that i_{lq} can indicate load reactive power demands since we have $\left(v_d \perp i_{lq}\right)$ in dq frame.

3. SYNCHRONOUS GENERATOR EMULATION CONTROL STRATEGY

Increased penetration of power electronic based generation units in the grid can lead to a serious decrease in system inertia. The frequency of such a system would be very sensitive to load or generation variations. Therefore, large deviations of frequency could possibly lead to system instability. In this regard, using VSCs in order to provide frequency support would be so beneficial from the frequency stability point of view. The theory of virtual inertia emulation by means of power electronic interfaces was first proposed by Beck and Hesse.[32] Since then, various approaches and topologies have been established which focus on providing inertial response, frequency regulation, and damping deviations.

The proposed virtual inertia emulation control strategy here includes the famous swing equation which can approximate frequency deviations of the system based on active power variations. In this regard, (15) can be expressed as follows:

$$P_{in} - P_{out} = J\omega_0 \frac{d\omega}{dt} + D\omega_0 \left(\omega - \omega_0\right) \tag{15}$$

where, P_{in} represents VSC's active power input, estimated by the governor model, and P_{out} represents converter's active power output which has been specified by the proposed controller in section II in order to supply load demands. In addition, J and D represent the virtual inertia and damping factors while ω and ω_0 are the virtual and reference values of the angular frequency. The controller computes ω_0 and P_{out} based on converter output current and PCC voltage measurements. As mentioned earlier, the governor characteristics of a SG are also included here in order to emulate a more SG like behavior. Demonstrated in Figure 2, the considered governor model used to estimate P_{in} consists of a droop controller coefficient (Kg) along with a mechanical delay (Tg).

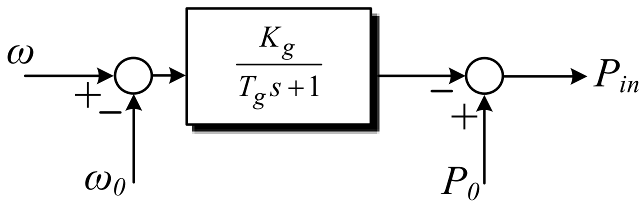

FIGURE 2. Schematic diagram of the emulated governor model.

Therefore, the governor model of a real SG can be emulated here in terms of a first order lag unit as:

$$P_0 - P_{in} = \frac{K_g}{T_g s + 1}\left(\omega - \omega_0\right) \tag{16}$$

where, P_0 represents the set value of load active power. In this regard, the total equation of the proposed virtual inertia emulation controller can be expressed as:

$$P_0 - \underbrace{\frac{K_g}{T_g s + 1}\left(\omega - \omega_0\right)}_{\varphi_\omega} - P_{out} = J\omega_0 \frac{d\omega}{dt} + D\omega_0 \left(\omega - \omega_0\right) \tag{17}$$

The general schematic diagram of the proposed controller is depicted in Figure 3. Within the proposed control strategy, there are two main control loops. The inner control loop utilizes dynamic equations of the grid-connected converter in order to provide a fast accurate compensation of load active and reactive power demands. In addition, the frequency equation represented by (17) is solved in every control period within the outer control loop in order to determine the appropriate phase command θ for the inner control loop. The proposed strategy can be considered as a simple yet practical solution for VSC's in order to emulate synchronous generator like behaviors.

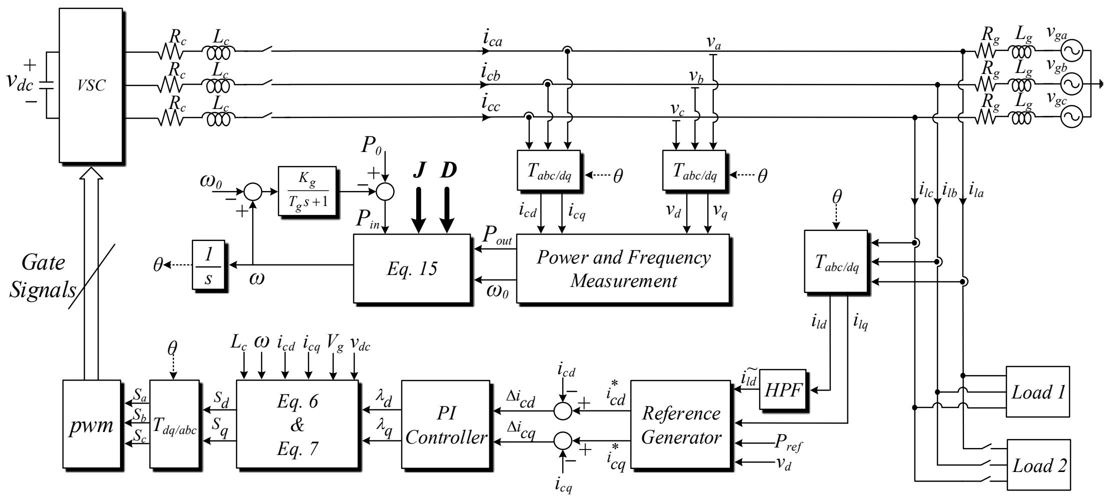

FIGURE 3. General schematic diagram of the proposed controller.

It should be noted that P_0, P_{out}, K_g, and T_g along with ω_0 are considered as the inputs to the proposed inertia emulation controller. Therefore, appropriate tuning of parameters J and D in this equation should be considered necessary in order to prevent oscillatory system performance. In this regard, relevant eigenvalue analysis of the controller can be useful in order to evaluate the effects of parameter dynamics on the stability studies.

Considering (17), any dynamics of converter's output active power defined as $\Delta P = P_0 - P_{out}$, will eventually result in frequency dynamics of $\Delta\omega = \omega - \omega_0$. In this regard, the transfer function from $\Delta\omega$ to ΔP can be extracted as:

$$\frac{\Delta\omega}{\Delta P} = \frac{1}{J\omega_0 s + D\omega_0 + \dfrac{K_g}{T_g s + 1}} = \frac{T_g s + 1}{J\omega_0 T_g s^2 + \left(J\omega_0 + D\omega_0 T_g\right)s + \left(D\omega_0 + K_g\right)} \tag{18}$$

Various dynamic conditions of the controller can now be described based on the eigenvalue analysis of this transfer function. Considering the $\omega_0 = 100\pi$ rad/s,

$K_g = 15 \times 10^5$, $T_g = 6$, $J = 3$, and variable D, the root locus analysis for the characteristic equation of the system has been demonstrated in Figure 4a. As it can be seen, minimum and maximum damping assignment can lead to oscillatory modes while in between, increasing the damping factor of the controller will result in a more stable operation as the transfer function poles are moving further away towards left of the imaginary axis. In this regard, time domain frequency responses of the system, considering 3 different damping values, have been demonstrated in Figure 4b. It should be noted that since the main objective of the simulations is to demonstrate the effect of the designed inertia controller on frequency dynamics, all simulation results are represented with a focus on load dynamics at t=2 seconds. In this regard, the demonstrated results in Figure 4b can confirm the abovementioned expectations that increasing the value of parameter D in the controller can lead to a more damped frequency response characteristic.

In addition, it is worth mentioning that every operating point on this modal trajectory of the system can offer a specific frequency response characteristic. This significant yet simple point will be further discussed in the next section where the eigenvalue trajectory of the system is utilized in order to design an automatic technique for controller parameter value adjustments.

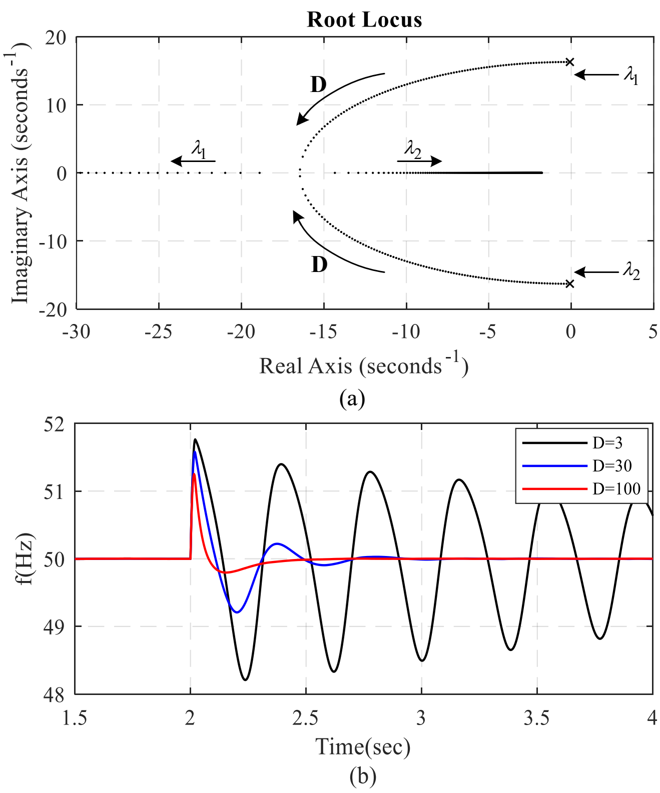

FIGURE 4. Damping variation impacts on system eigenvalues: (a) root locus trajectory, and (b) time domain frequency dynamics considering various D values.

4. PROPOSED CONTROLLER DESIGN AND STATE-SPACE ANALYSIS

This section provides the underlying concepts of the proposed method and then, describes the designed control algorithm. In addition to that, state-space stability analysis has also been provided here in order to demonstrate the superiority of the proposed control method over the conventional structures.

4.1 Proposed Controller Design

In order to investigate the impacts of various parameter values on small signal stability of the system, root locus trajectory of the controller has been demonstrated in Figure 5. Considering $1 \leq J \leq 10$ and $0 \leq D \leq 500$, a variety of operating points are provided. As mentioned before, each operating point on this eigenvalue trajectory of the controller can lead to a specific frequency dynamic response since it provides a particular damping ratio (ξ) and natural frequency (ω_n) characteristic.

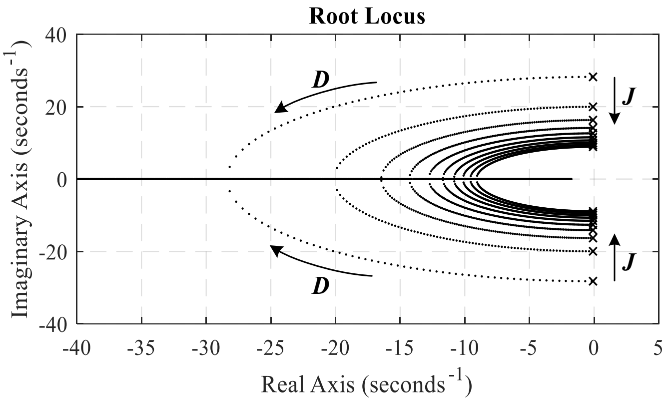

FIGURE 5. Root locus trajectory of the controller considering various inertia and damping coefficients.

This valuable inherent potential of the root locus trajectory can then be used in controller design. Considering the flow chart of the proposed controller represented in Figure 6, inertia and damping coefficients of the controller can be automatically adjusted based on the desired frequency response characteristic.

Considering the proposed controller algorithm, a maximum damping ratio of $\xi = 1$ can be provided in order to have an over-damped frequency dynamic while necessary. However, various studies suggest that an approximate damping ratio of $\xi = 0.5$ can lead to a more flexible interaction between VSG and the power grid and thus should be considered in stability assessments.[33]

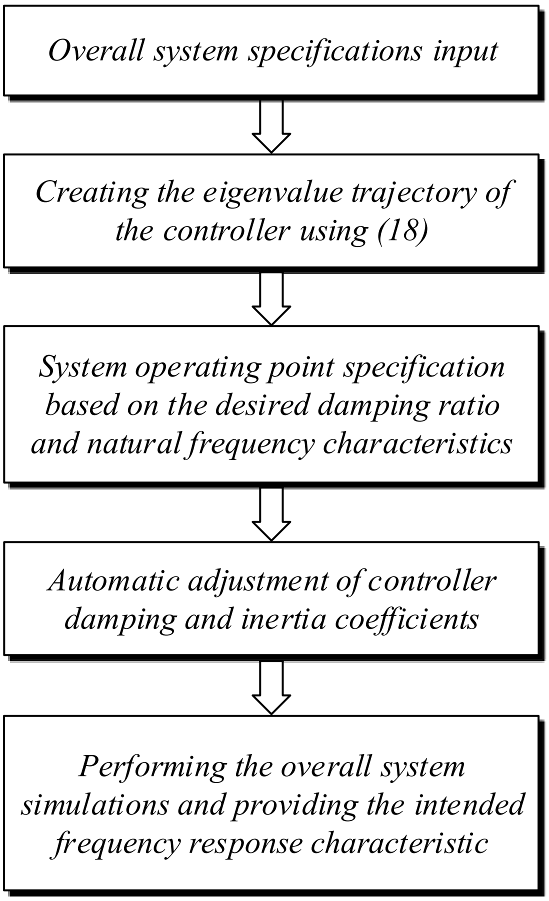

FIGURE 6. Flow chart of the proposed controller algorithm for automatic adjusment of the VSG parameters.

4.2 State-Space Stability Analysis

In order to demonstrate the superiority of the proposed control method over conventional structures, state-space analysis has been utilized here. As literature shows, the majority of inertia-less control structures use phase-locked loop (PLL) as an interaction method to properly synchronize the converter to the grid. In this regard, the PLL dynamics can often be described as a second-order filter with K_{ppll} and K_{ipll} coefficients, applied on PCC voltages. Therefore, the state-space equation of the PLL can be expressed as:

$$\dot{\theta} = \omega = \omega_0 + K_{ppll} v_q + \underbrace{K_{ipll} \int v_q dt}_{\varphi_\theta} \tag{19}$$

where $\dot{\theta}$ is the derivative of the phase command θ. On the other hand, applying KVL to the grid side of the structure represented in Figure 1 leads to:

$$\frac{d}{dt}\begin{bmatrix} i_{gd} \\ i_{gq} \end{bmatrix} = \frac{1}{L_g}\begin{bmatrix} v_{gd} \\ v_{gq} \end{bmatrix} - \begin{bmatrix} \frac{R_g}{L_g} & -\omega \\ \omega & \frac{R_g}{L_g} \end{bmatrix}\begin{bmatrix} i_{gd} \\ i_{gq} \end{bmatrix} - \frac{1}{L_g}\begin{bmatrix} v_d \\ v_q \end{bmatrix} \tag{20}$$

Therefore, the state equations (4)-(9) as well as (19)-(20) can be linearized around the equilibrium points (noted by subscripts 0) in order to provide the stability assessment studies based on small signal state-space analysis of the system as follows:

$$\begin{bmatrix} \Delta \dot{x}_{conv} \end{bmatrix} = \begin{bmatrix} A_{conv} \end{bmatrix}\begin{bmatrix} \Delta x_{conv} \end{bmatrix} + \begin{bmatrix} B_{conv} \end{bmatrix}\begin{bmatrix} \Delta u \end{bmatrix} \tag{21}$$

where the prefix Δ represents the small variations of each state variable around the equilibrium point and the subscript $conv$ refers to the utilization of conventional methods, meaning PLL. Also, the state matrix Δx_{conv} and the input matrix Δu are expressed as follows:

$$\Delta x_{conv} = \begin{bmatrix} \Delta\theta \ \Delta\varphi_\theta \ \Delta i_{cd} \ \Delta i_{cq} \ \Delta\varphi_{i_{cd}} \ \Delta\varphi_{i_{cq}} \ \Delta i_{gd} \ \Delta i_{gq} \end{bmatrix} \tag{22}$$

$$\Delta u = \begin{bmatrix} \Delta P_{in} \ \Delta Q_{in} \end{bmatrix} \tag{23}$$

It should be noted that the state variables $\Delta\varphi_\theta$, $\Delta\varphi_{i_{cd}}$, and $\Delta\varphi_{i_{cq}}$ are associated with the integral parts of the abovementioned PLL and the PI current controllers. The state and input matrices of the conventional system are represented in detail in Appendix.

The same procedure can be applied on the proposed controller, using virtual inertia. In this regard, the state equation (17) will be studied instead of (19) and the state variables $\Delta\theta$ and $\Delta\varphi_\theta$ will be replaced with $\Delta\omega$ and $\Delta\varphi_\omega$, respectively. This state-space realization of the proposed controller (represented with the subscript pro) have also been provided in Appendix.

The stability assessments are analyzed according to the sensitivity of the controller eigenvalues with regards to the parameter variations. With that in mind, Figure 7 depicts the eigenvalue trajectory of both conventional and proposed controllers. Each trajectory can be studied for 8 different modes which are marked with numbers. Figure 7a illustrates the first case study based on the conventional structure where K_{ppll} has been modified. In this regard, the modification of the PLL parameter significantly affects the modes 6,7, and 8 while, its impact on the other poles can be neglected. It should be noted that considering the Lyapunov stability theory, the conventional structure demonstrates potential instabilities as one pole (mode 8) is moving towards the positive side of the s-plane, known as the unstable region.

On the other hand, Figure 7b demonstrates the second case study where the inertia parameter has been modified in the proposed structure. In this regard, two modes of 5 and 8 have been moved towards the left-hand side of the imaginary axis while, other poles are remained almost unaffected. It is worth mentioning that the movement of mode 8 to the axis origin point has yield to a none-positive trajectory which is mostly moving towards the left-hand side of the axis and therefore, the system has become stable using the proposed control structure.

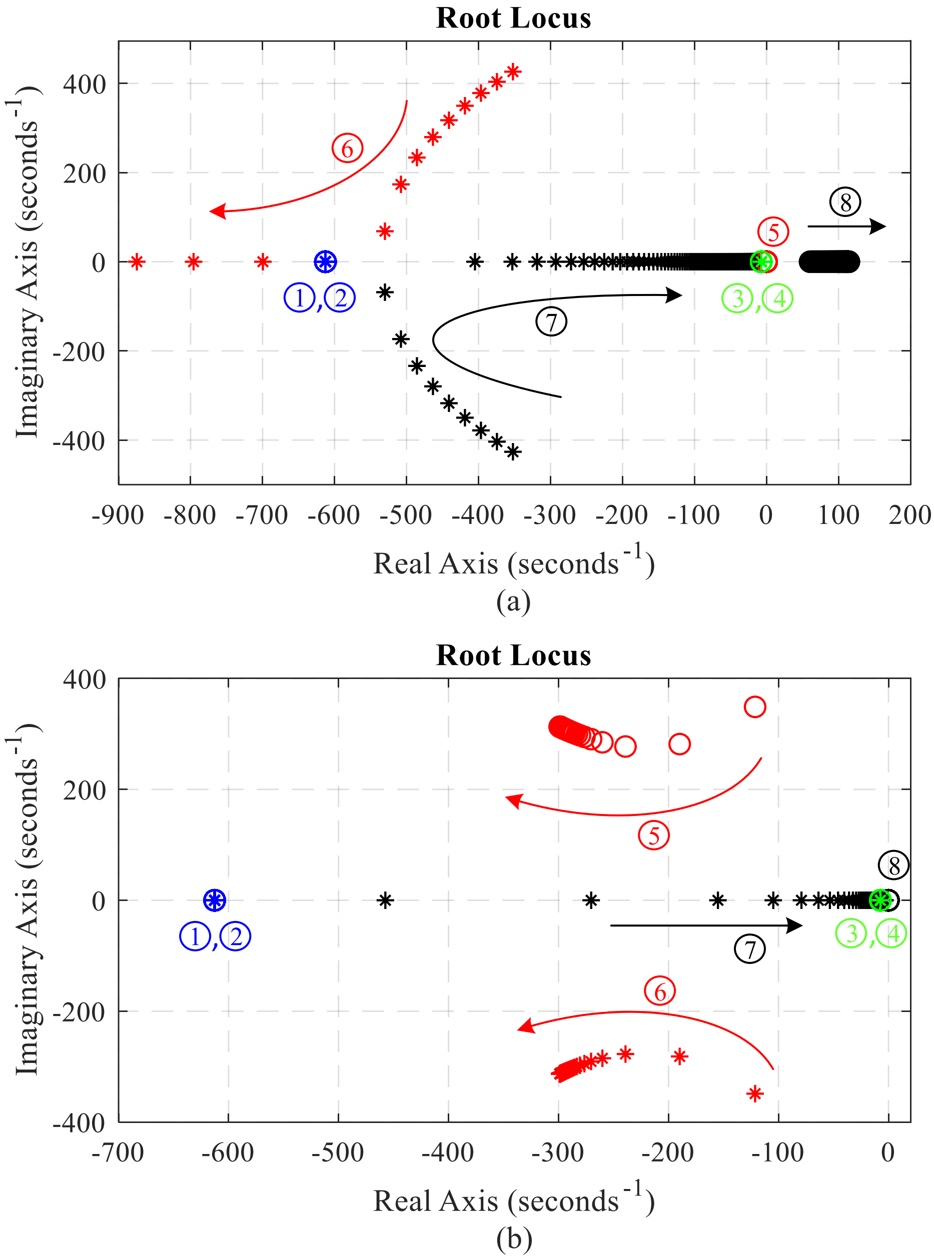

FIGURE 7. The eigenvalue analysis of the system: (a) conventional structure with modification of PLL parameters, (b)proposed structure with modification of inertia.

5. SIMULATION RESULTS AND DISCUSSION

In order to evaluate the efficient operation of the proposed controller, the detailed model demonstrated in Figure 3 has been simulated in MATLAB/Simulink. Various circuit component values along with the operational conditions of the simulations are given in Table 1.

TABLE 1. Parameter values and operational conditions applied to simulations

Items	Values
dc-link voltage v_{dc}	40 KV
Grid voltage (V_g) (L-L,rms)	13.8 KV
Equivalent resistance between converter and PCC (R_c)	0.1 Ω
Equivalent inductance between converter and PCC (L_c)	3 mH
Grid resistance (R_g)	0.1 Ω
Grid inductance (L_g)	0.01 mH
System frequency (f)	50 Hz
Switching/Sampling frequency	10 KHz
Load1 active power (P_{ref})	16 MW
Load1 reactive power	10 MVar

Two simulation scenarios are studied here. The initial scenario focuses on active and reactive power compensation capabilities of the proposed method while the second one studies virtual inertia emulation proficiencies in detail. In this regard, Figure 8 shows load, grid, and converter currents. As it can be seen, before 2 seconds converter is connected, compensating all load active and reactive power demands with fast accurate dynamics. Then at 2 seconds, second load is connected which has the same power demands as the first load. Since VSC has a maximum limit for its output power, converter current references are adjusted such that maximum available active power (P_{ref}) and complete reactive power demands of the load are compensated. In this regard, grid current remains sinusoidal and also in-phase with grid voltage as shown in Figure 8d.

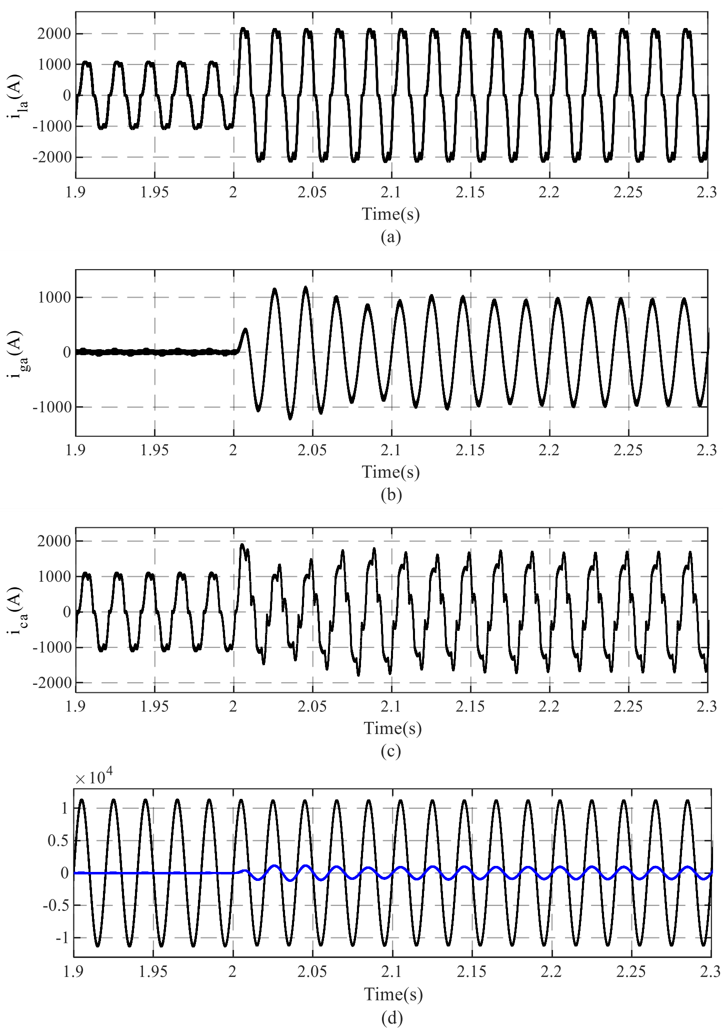

FIGURE 8. Simulated waveforms of the proposed VSC: (a) phase-a waveform of load current, (b) phase-a waveform of grid current, (c) phase-a waveform of converter output current, and (d) simulated waveforms of grid voltage and current.

In order to evaluate inertia emulation capabilities of the proposed VSC, minor changes have been applied to the first simulation scenario. In this regard, maximum available active power of the converter has been increased in order to guarantee an effective supply of total load active power demands. Therefore, as it can be concluded from (15), the connection of a second load at 2 seconds increases output power of the converter and thus leads to a frequency dynamic. In order to demonstrate the enhanced dynamic frequency responses of the proposed algorithm, a comparative study between the proposed inertia-based control method and the conventional PLL-based controllers of the VSCs has been considered hereafter. Demonstrated in Figure 9, the comparisons between frequency responses provided by the conventional PLL-based controllers and the proposed virtual inertia algorithm clearly denote the superior dynamic behavior of the latter.

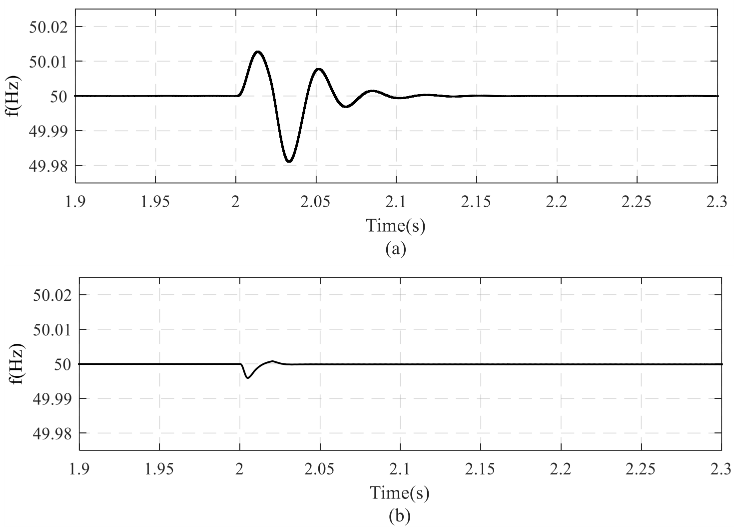

FIGURE 9. Dynamic frequency responses of the system provided by: (a) PLL, and (b) proposed virtual inertia algorithm.

As mentioned before, every point on the root locus trajectory provides a specific frequency response characteristic based on its damping ratio and natural frequency. In this regard, two different operating points have been considered in order to evaluate the accurate performance of the proposed controller. The first operating point is considered to provide an overdamped frequency dynamic ($\xi = 1$) while the second one provides a more flexible frequency response ($\xi = 0.5$). In addition to that, considering a settling time (T_s) of 0.7 second will result in the $\omega_n = 6$ and 12 rad/s respectively, since $T_s \approx 4 / \xi\omega_n$. Therefore, demonstrated in Figure 10, the abovementioned operating points have been automatically chosen by the proposed control algorithm based on the desired frequency response characteristics. Then, applying the values of damping and inertia coefficients provided by the proposed control algorithm, time domain frequency dynamic simulation results have been obtained as shown in Figure 11. As it can be seen, the desired overdamped frequency dynamic as well as the appropriate flexible frequency response have been perfectly provided.

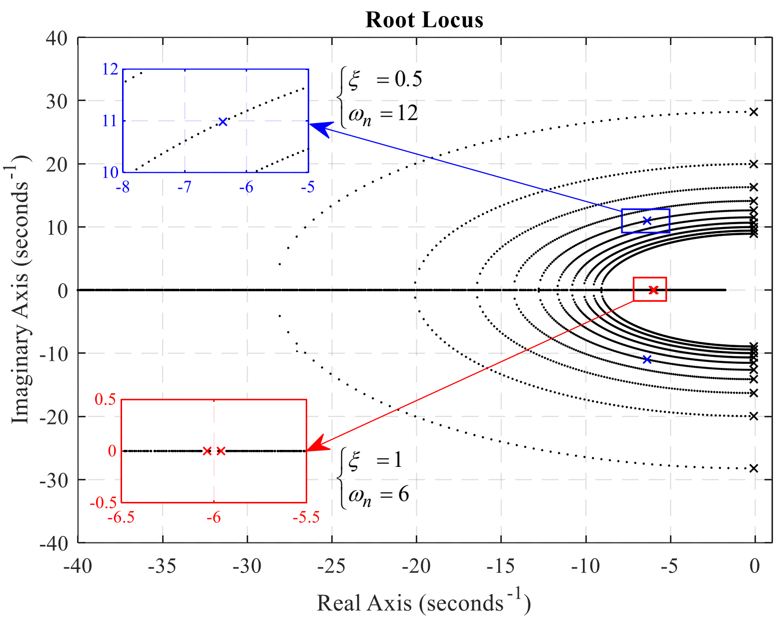

FIGURE 10. Automatic detection of the desired operating points based on the given frequency response charactristics.

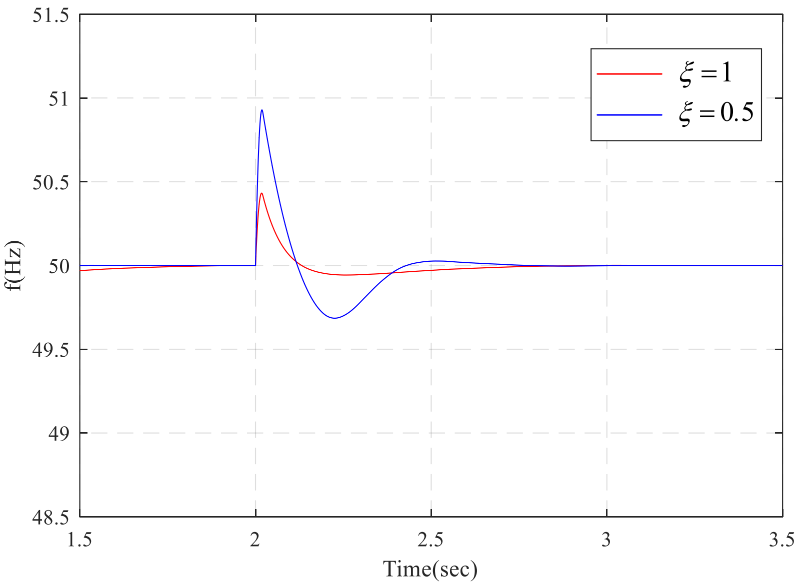

FIGURE 11. Frequency dynamics of the proposed controller considering two different frequency response charactristics.

It should be noted that using the proposed inertia emulation strategy, the converter could act similar to a SG and thus, total inertia of the power system is improved. In addition, inappropriate tuning of virtual inertia and damping factor parameters can lead to an oscillatory dynamic frequency response which can even result in frequency instabilities if major power deviations happen in the system. Therefore, auto adjustment of the control parameters based on a desired frequency response characteristic can guarantee the stable performance of the controller as well.

6. CONCLUSION

This paper presented an enhanced control method for VCSs, considering virtual inertia emulation strategy. Dynamic behavior of the proposed converter has been studied in order to demonstrate its active and reactive power compensation capabilities. Considering the limitations of the maximum available active power of the converter, simulation results show an accurate, fast dynamic response of the proposed method while successfully providing load power demands. In addition to that, a virtual inertia based control strategy has been proposed based on the eigenvalue analysis of the controller parameters. Reflecting the power deviations in dynamic system frequency response, this method provides a SG like behavior using VSCs as well as an auto adjustment capability of controller parameters based on a desired frequency response characteristic. The proposed controller can be considered as a simple yet beneficial solution to the reduced power system inertia related issues.

ACKNOWLEDGMENTS

This work was supported by the Babol Noshirvani University of Technology under Grant BNUT/389051/99.

CONFLICT OF INTEREST STATEMENT

The authors have no conflict of interest to declare.

REFERENCES

1. European Committee of the Regions. EU Energy System Integration Strategy [Fact Sheet]. European Commission; 2020. https://ec.europa.eu/commission/presscorner/detail/en/fs_20_1295
2. Cao Y, Wang W, Li Y, et al. A virtual synchronous generator control strategy for VSC-MTDC systems. IEEE trans energy convers. 2018;33(2):750-761.
3. Zheng T, Chen L, Guo Y, Mei S. Comprehensive control strategy of virtual synchronous generator under unbalanced voltage conditions. IET Gener Transm Distrib. 2018;12(7):1621-1630.
4. Shahnazian F, Adabi J, Pouresmaeil E, Catalão JPS. Interfacing modular multilevel converters for grid integration of renewable energy sources. Electric Power Syst Res. 2018;160:439-449.

5. Pouresmaeil E, Montesinos-Miracle D, Gomis-Bellmunt O. Control scheme of three-level NPC inverter for integration of renewable energy resources into AC grid. IEEE Syst J. 2012;6(2):242-253.
6. Rosso R, Wang X, Liserre M, Lu X, Engelken S. Grid-Forming Converters: Control Approaches, Grid-Synchronization, and Future Trends—A Review. IEEE Open Journal of Industry Applications. 2021;2:93-109. doi:10.1109/ojia.2021.3074028
7. Adineh B, Keypour R, Davari P, Blaabjerg F. Review of Harmonic Mitigation Methods in Microgrid: From a Hierarchical Control Perspective. IEEE Journal of Emerging and Selected Topics in Power Electronics. 2021;9(3):3044-3060. doi:10.1109/jestpe.2020.3001971
8. Huang L, Wu C, Zhou D, Blaabjerg F. Grid Impedance Impact on the Maximum Power Transfer Capability of Grid-Connected Inverter. 2021 IEEE 12th Energy Conversion Congress & Exposition - Asia (ECCE-Asia). Published online May 24, 2021. doi:10.1109/ecce-asia49820.2021.9479080
9. Taul MG, Wu C, Chou S-F, Blaabjerg F. Optimal Controller Design for Transient Stability Enhancement of Grid-Following Converters Under Weak-Grid Conditions. IEEE Transactions on Power Electronics. 2021;36(9):10251-10264. doi:10.1109/tpel.2021.3066205
10. Pouresmaeil E, Miguel-Espinar C, Massot-Campos M, Montesinos-Miracle D, Gomis-Bellmunt O. A control technique for integration of DG units to the electrical networks. IEEE Trans Ind Electron. 2013;60(7):2881-2893.
11. Mehrasa M, Pouresmaeil E, Soltani H, Blaabjerg F, Calado M, Catalão J. Virtual inertia and mechanical power-based control strategy to provide stable grid operation under high renewables penetration. Appl Sci (Basel). 2019;9(6):1043.
12. Khan S, Bletterie B, Anta A, Gawlik W. On small signal frequency stability under virtual inertia and the role of PLLs. Energies. 2018;11(9):1-18.
13. Rakhshani E, Rodriguez P. Inertia emulation in AC/DC interconnected power systems using derivative technique considering frequency measurement effects. IEEE Trans Power Syst. 2017;32(5):3338-3351.
14. Tamrakar U, Shrestha D, Maharjan M, Bhattarai B, Hansen T, Tonkoski R. Virtual inertia: Current trends and future directions. Appl Sci (Basel). 2017;7(7):654.
15. Xu Q, Dragicevic T, Xie L, Blaabjerg F. Artificial Intelligence-Based Control Design for Reliable Virtual Synchronous Generators. IEEE Transactions on Power Electronics. 2021;36(8):9453-9464. doi:10.1109/tpel.2021.3050197

16. Poolla BK, Gros D, Dorfler F. Placement and implementation of grid-forming and grid-following virtual inertia and fast frequency response. IEEE Trans Power Syst. 2019;34(4):3035-3046.
17. Kerdphol T, Rahman FS, Watanabe M, Mitani Y. Robust virtual inertia control of a low inertia microgrid considering frequency measurement effects. IEEE Access. 2019;7:57550-57560.
18. Ashabani M, Jung J. Synchronous voltage controllers: Voltage-based emulation of synchronous machines for the integration of renewable energy sources. IEEE Access. 2020;8:49497-49508.
19. Sun D, Liu H, Gao S, Wu L, Song P, Wang X. Comparison of Different Virtual Inertia Control Methods for Inverter-based Generators. Journal of Modern Power Systems and Clean Energy. 2020;8(4):768-777. doi:10.35833/mpce.2019.000330
20. Wang Y, Wang C, Xu L, Meng J, Hei Y. Adjustable inertial response from the converter with adaptive droop control in DC grids. IEEE Trans Smart Grid. 2019;10(3):3198-3209.
21. Meng X, Liu J, Liu Z. A generalized droop control for grid-supporting inverter based on comparison between traditional droop control and virtual synchronous generator control. IEEE Trans Power Electron. 2019;34(6):5416-5438.
22. Zhao F, Shuai Z, Shen C, Cheng H, Shen Y, Peng Y. Comparison of Transient Angle Stability Between Virtual Synchronous Generator and Droop-controlled Inverter. 2020 IEEE Applied Power Electronics Conference and Exposition (APEC). Published online March 2020. doi:10.1109/apec39645.2020.9124158
23. Torres M, Lopes LAC. Virtual synchronous generator: A control strategy to improve dynamic frequency control in autonomous power systems. Energy Power Eng. 2013;05(02):32-38.
24. Xiong X, Wu C, Cheng P, Blaabjerg F. An Optimal Damping Design of Virtual Synchronous Generators for Transient Stability Enhancement. IEEE Transactions on Power Electronics. 2021;36(10):11026-11030. doi:10.1109/tpel.2021.3074027
25. Jongudomkarn J, Liu J, Ise T. Virtual Synchronous Generator Control with Reliable Fault Ride-Through Ability: A Solution Based on Finite-Set Model Predictive Control. IEEE Journal of Emerging and Selected Topics in Power Electronics. 2020;8(4):3811-3824. doi:10.1109/jestpe.2019.2942943
26. Moulichon A, Alamir M, Debusschere V, et al. Observer-Based Current Controller for Virtual Synchronous Generator in Presence of Unknown and Unpredictable

Loads. IEEE Transactions on Power Electronics. 2021;36(2):1708-1716. doi:10.1109/tpel.2020.3010085

27. Wang Z, Zhuo F, Yi H, Wu J, Wang F, Zeng Z. Analysis of dynamic frequency performance among voltage-controlled inverters considering virtual inertia interaction in microgrid. IEEE Trans Ind Appl. 2019;55(4):4135-4144.
28. Ebrahimi M, Khajehoddin SA, Karimi-Ghartemani M. An improved damping method for virtual synchronous machines. IEEE Trans Sustain Energy. 2019;10(3):1491-1500.
29. Priyamvada IRS, Das S. Impact of PLL on Harmonic Stability of Renewable Dominated Power System: Modeling and Analysis. 2018 IEEE International Conference on Power Electronics, Drives and Energy Systems (PEDES). Published online December 2018. doi:10.1109/pedes.2018.8707592
30. Kerdphol T, Rahman FS, Watanabe M, Mitani Y, Turschner D, Beck H-P. Enhanced virtual inertia control based on derivative technique to emulate simultaneous inertia and damping properties for microgrid frequency regulation. IEEE Access. 2019;7:1-1.
31. Kouki M, Marinescu B, Xavier F. Exhaustive Modal Analysis of Interconnected European Power System. 2020 IEEE Electric Power and Energy Conference (EPEC). Published online November 9, 2020. doi:10.1109/epec48502.2020.9320043
32. Beck H-P, Hesse R. Virtual synchronous machine. In: 2007 9th International Conference on Electrical Power Quality and Utilisation. IEEE Xplore; 2007:1-6.
33. Abdollahi M, Candela JI, Rocabert J, Munoz Aguilar RS, Hermoso JR. Synchronous power controller merits for dynamic stability improvement in long line by renewables. In: 2016 IEEE International Conference on Renewable Energy Research and Applications (ICRERA). IEEE; 2016:760-765.

APPENDIX

The state and input matrices associated with both conventional and proposed structures are provided as follows:

$$A_{conv} = \begin{bmatrix} 0 & 1 & K_{ppll}C' & K_{ppll}D' & 0 & 0 & K_{ppll}C' & K_{ppll}D' \\ 0 & 0 & K_{ipll}C' & K_{ipll}D' & 0 & 0 & K_{ipll}C' & K_{ipll}D' \\ 0 & 0 & -\left(\frac{K_p + R_c}{L_c}\right) & 0 & \frac{1}{L_c} & 0 & 0 & 0 \\ 0 & 0 & 0 & -\left(\frac{K_p + R_c}{L_c}\right) & 0 & \frac{1}{L_c} & 0 & 0 \\ 0 & 0 & -K_i & 0 & 0 & 0 & 0 & 0 \\ 0 & 0 & 0 & -K_i & 0 & 0 & 0 & 0 \\ 0 & I_{gq0} & -\frac{1}{L_g}C + I_{gq0}K_{ppll}C' & -\frac{1}{L_g}D + I_{gq0}K_{ppll}D' & 0 & 0 & -\frac{1}{L_g}C - \frac{R_g}{L_g} + I_{gq0}K_{ppll}C' & -\frac{1}{L_g}D + \omega_0 + I_{gq0}K_{ppll}D' \\ 0 & -I_{gd0} & -\left(\frac{1}{L_g} + I_{gd0}K_{ppll}\right)C' & -\left(\frac{1}{L_g} + I_{gd0}K_{ppll}\right)D' & 0 & 0 & -\left(\frac{1}{L_g} + I_{gd0}K_{ppll}\right)C' - \omega_0 & -\left(\frac{1}{L_g} + I_{gd0}K_{ppll}\right)D' - \frac{R_g}{L_g} \end{bmatrix}$$

$$A_{pro} = \begin{bmatrix} -\frac{D}{J} & -\frac{1}{J\omega_0} & -\frac{1}{J\omega_0}\left(v_{d0} + I_{cd0}C + I_{cq0}C'\right) & -\frac{1}{J\omega_0}\left(v_{q0} + I_{cd0}D + I_{cq0}D'\right) & 0 & 0 & -\frac{1}{J\omega_0}\left(I_{cd0}C + I_{cq0}C'\right) & -\frac{1}{J\omega_0}\left(I_{cd0}D + I_{cq0}D'\right) \\ \frac{K_g}{T_g} & -\frac{1}{T_g} & 0 & 0 & 0 & 0 & 0 & 0 \\ 0 & 0 & -\left(\frac{K_p + R_c}{L_c}\right) & 0 & \frac{1}{L_c} & 0 & 0 & 0 \\ 0 & 0 & 0 & -\left(\frac{K_p + R_c}{L_c}\right) & 0 & \frac{1}{L_c} & 0 & 0 \\ 0 & 0 & -K_i & 0 & 0 & 0 & 0 & 0 \\ 0 & 0 & 0 & -K_i & 0 & 0 & 0 & 0 \\ I_{gq0} & 0 & -\frac{1}{L_g}C & -\frac{1}{L_g}D & 0 & 0 & -\frac{1}{L_g}C - \frac{R_g}{L_g} & -\frac{1}{L_g}D + \omega_0 \\ -I_{gd0} & 0 & -\frac{1}{L_g}C' & -\frac{1}{L_g}D' & 0 & 0 & -\frac{1}{L_g}C' - \omega_0 & -\frac{1}{L_g}D' - \frac{R_g}{L_g} \end{bmatrix}$$

$$B_{conv} = \begin{bmatrix} K_{ppll}A' & K_{ppll}B' \\ K_{ipll}A' & K_{ipll}B' \\ 0 & 0 \\ 0 & 0 \\ 0 & 0 \\ 0 & 0 \\ -\frac{1}{L_g}A + I_{gq0}K_{ppll}A' & -\frac{1}{L_g}B + I_{gq0}K_{ppll}B' \\ -\left(\frac{1}{L_g} + I_{gd0}K_{ppll}\right)A' & -\left(\frac{1}{L_g} + I_{gd0}K_{ppll}\right)B' \end{bmatrix}, \quad B_{pro} = \begin{bmatrix} 0 & 0 \\ 0 & 0 \\ 0 & 0 \\ 0 & 0 \\ 0 & 0 \\ 0 & 0 \\ -\frac{1}{L_g}A & -\frac{1}{L_g}B \\ -\frac{1}{L_g}A' & -\frac{1}{L_g}B' \end{bmatrix}$$

where,

$$A = \frac{I_{d0}}{I_{d0}^2 + I_{q0}^2}, B = \frac{I_{q0}}{I_{d0}^2 + I_{q0}^2}, C = \frac{v_{q0}I_{q0} - v_{d0}I_{d0}}{I_{d0}^2 + I_{q0}^2}, D = -\frac{v_{d0}I_{q0} + v_{q0}I_{d0}}{I_{d0}^2 + I_{q0}^2}$$

$$A' = \frac{I_{q0}}{I_{d0}^2 + I_{q0}^2}, B' = -\frac{I_{d0}}{I_{d0}^2 + I_{q0}^2}, C' = -\frac{v_{d0}I_{q0} + v_{q0}I_{d0}}{I_{d0}^2 + I_{q0}^2}, D' = \frac{v_{d0}I_{d0} - v_{q0}I_{q0}}{I_{d0}^2 + I_{q0}^2}$$

and $\begin{cases} i_d = i_{cd} + i_{gd} \\ i_q = i_{cq} + i_{gq} \end{cases}$.